Source shape estimation for neutron imaging systems using convolutional neural networks

Saavedra, Gary Joseph; Geppert-Kleinrath, Verena; Danly, Christopher Russell; Durocher, Mora; Wilde, Carl Huerstel; Fatherley, Valerie E.; Mendoza, Emily Faith; Tafoya, Landon Reese; Volegov, Petr; Fittinghoff, David; Rubery, Michael; Freeman, Matthew Stouten

To be published in: Review of Scientific Instruments

DOI to publisher's version: 10.1063/5.0214449

Review of Scientific Instruments

RESEARCH ARTICLE | AUGUST 29 2024

Source shape estimation for neutron imaging systems using convolutional neural networks

Special Collection: Proceedings of the 25th Topical Conference on High-Temperature Plasma Diagnostics

Gary Saavedra ; Verena Geppert-Kleinrath ; Chris Danly ; Mora Durocher ; Carl Wilde ; Valerie Fatherley ; Emily Mendoza; Landon Tafoya ; Petr Volegov ; David Fittinghoff ; Michael Rubery ; Matthew S. Freeman

Rev. Sci. Instrum. 95, 083559 (2024)
https://doi.org/10.1063/5.0214449

AIP Publishing

Review of Scientific Instruments ARTICLE pubs.aip.org/aip/rsi

Source shape estimation for neutron imaging systems using convolutional neural networks

Cite as: Rev. Sci. Instrum. 95, 083559 (2024); doi: 10.1063/5.0214449
Submitted: 17 April 2024 • Accepted: 8 August 2024 •
Published Online: 29 August 2024

Gary Saavedra,[1,a)] Verena Geppert-Kleinrath,[1] Chris Danly,[1] Mora Durocher,[1] Carl Wilde,[1] Valerie Fatherley,[1] Emily Mendoza,[1] Landon Tafoya,[1] Petr Volegov,[2] David Fittinghoff,[2] Michael Rubery,[2] and Matthew S. Freeman[1]

AFFILIATIONS

[1] Los Alamos National Laboratory, Los Alamos, New Mexico 87544, USA
[2] Lawrence Livermore National Laboratory, Livermore, California 94550, USA

Note: This paper is part of the Special Topic on Proceedings of the 25th Topical Conference on High-Temperature Plasma Diagnostics.
[a)]**Author to whom correspondence should be addressed:** gsaavedra@lanl.gov

ABSTRACT

Neutron imaging systems are important diagnostic tools for characterizing the physics of inertial confinement fusion reactions at the National Ignition Facility (NIF). In particular, neutron images give diagnostic information on the size, symmetry, and shape of the fusion hot spot and surrounding cold fuel. Images are formed via collection of neutron flux from the source using a system of aperture arrays and scintillator-based detectors. Currently, reconstruction of fusion source geometry from the collected neutron images is accomplished by solving a computationally intensive maximum likelihood estimation problem via expectation maximization. In contrast, it is often useful to have simple representations of the overall source geometry that can be computed quickly. In this work, we develop convolutional neural networks (CNNs) to reconstruct the outer contours of simple source geometries. We compare the performance of the CNN for penumbral and pinhole data and provide experimental demonstrations of our methods on both non-noisy and noisy data.

I. INTRODUCTION

Recently, the National Ignition Facility (NIF) at the Lawrence Livermore National Laboratory successfully attained thermonuclear ignition, a milestone supported significantly by an array of diagnostics.[1] Critical among these tools is the neutron imaging system (NIS), which is instrumental in analyzing the fusion reaction's geometry.[2] The fusion source images reconstructed by using this system provide essential details about the fusion hot spot's size, symmetry, and shape, as well as the surrounding cold fuel. These images have been indispensable for inertial confinement fusion (ICF) research, including groundbreaking experiments that have led to ignition.

The NIS uses a solid gold array consisting of large circular and semi-circular penumbra, as well as small triangular pinholes, as shown in Fig. 1(a). The penumbra is used primarily for pointing, while the pinholes are used for finer shape reconstruction details. Neutrons in the 14 MeV range are ejected from the implosion hot spot and pass through the array to a scintillator-based detection system to generate a neutron aperture image.[3] Due to the long mean-interaction length of neutrons, the aperture array is elongated to ~20 cm, as shown in Fig. 1(b), to ensure only neutrons that have passed through the penumbra or pinholes are detected.

The NIS reconstructs source geometries from the neutron aperture image via an iterative Bayesian approach.[4] A key component of this reconstruction is finding an elliptical contour that approximates the overall shape of the source. In addition to giving important information about the overall size and shape, the elliptical contour aids in determining source location within the field of view, as well as diagnosing the quality of the full pixel-by-pixel reconstruction. In this paper, we develop an approach using deep neural networks (DNNs) to predict the elliptical contour. In particular, we train a convolutional neural network (CNN) to predict the major and minor axes size of the ellipse from a neutron aperture image.

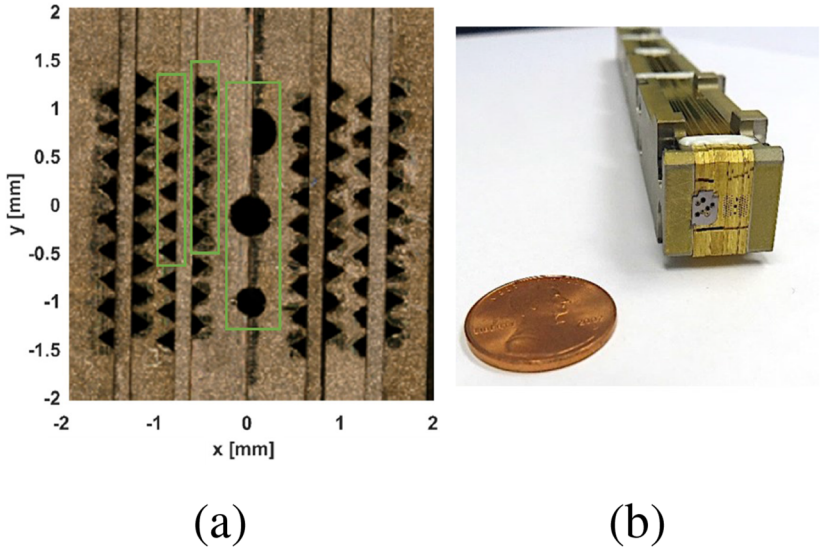

FIG. 1. (a) Front-face view of the NIS-3 aperture. This array contains 3 semi-circular penumbra and 72 triangular apertures. The apertures within the green boxes were used in this study. (b) Depth-wise view of the NIS-3 aperture.

CNNs have transformed the realm of image processing, showcasing their capability to learn from extensive datasets.[5] Unlike traditional image processing methods that depend on manually crafted features—restricting their adaptability and increasing the time humans must invest—CNNs demand less time from analysts and in certain cases can be more accurate. Furthermore, they often require less computation time when making predictions compared to other algorithms. For more information on comparison between CNNs and hand-crafted image processing techniques, see Refs. 6–8.

We show that CNNs can create fast and accurate approximations of these elliptical contours. CNNs consist of a set of convolution filters that determine spatially relevant features within an image. These features are then passed into a feedforward neural network for prediction. See the work by Goodfellow *et al.*[9] for a more detailed introduction to CNNs.

II. SOURCE RECONSTRUCTION

In an ICF experiment, the NIS diagnostic generates an aperture image as shown in Fig. 2(a). To create an image of the fusion source as shown in Fig. 2(b), a suite of iterative Bayesian inference algorithms processes the aperture image. The source is reconstructed

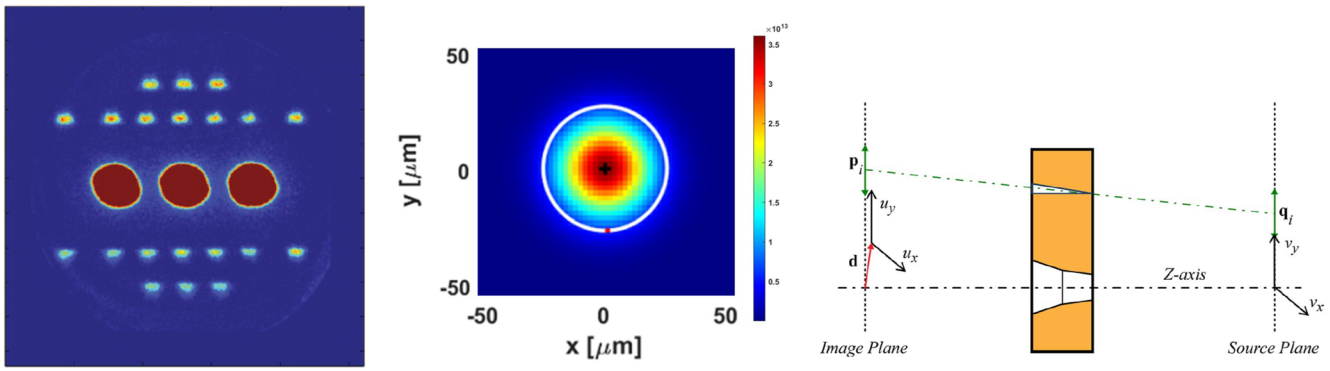

FIG. 2. (a) Example of a neutron aperture image, *I*, produced by aperture array for line-of-sight NIS-1. (b) Example of a reconstructed circular source distribution *S* with radius 25 μm. Color intensity represents neutrons per pixel. (c) Coordinate system notation (not to scale). Figures in panels (a) and (c) are reproduced with permission from Volegov *et al.*, Rev. Sci. Instrum. **85**, 023508 (2014). Copyright 2014 AIP Publishing LLC and Rev. Sci. Instrum. **85**, 123506 (2014). Copyright 2014 AIP Publishing LLC.

over three nearly orthogonal lines of sight, enabling the observation of the source from multiple perspectives.

Considering a source denoted as S and an aperture point spread function represented by K, the aperture image I, captured by the detector, is expressed as

$$I(\mathbf{u}) = \sum_{i=1}^{N_a} \int_V K_i(\mathbf{u} - \mathbf{p}_i + \mathbf{d}, \mathbf{v} - \mathbf{q}_i) S(\mathbf{v}) \partial^2 v. \quad (1)$$

In this formula, N_a signifies the total count of apertures, $\mathbf{d}$ represents the scintillator's center, and $\mathbf{p}_i$ along with $\mathbf{q}_i$ denote the coordinates of aperture i's central axis on the detector and source planes, respectively. The vectors $\mathbf{u}$ and $\mathbf{v}$ designate positions within the detector and source planes, respectively [refer to Fig. 2(c)].

In addition to a full reconstruction, it is often useful to create a simpler reconstruction that gives general shape characteristics for the source. For this purpose, we create simple elliptical reconstructions that approximate the shape of the outer contour of the source. An example of an outer contour is shown by the white circle in Fig. 2(b). These elliptical reconstructions serve several purposes. First, the elliptical reconstruction is computationally cheaper than the full reconstruction and allows for a quick look at the source shape. Second, the elliptical reconstruction can be used to diagnose and confirm the accuracy of the full reconstruction by comparing general shape characteristics. Third, the elliptical reconstruction is used in improving and understanding the metrology of the apertures.[10]

III. EXPERIMENTAL RESULTS

A. Dataset and preprocessing

Our objective is to employ a CNN to predict an elliptical source contour from the neutron aperture image. For this purpose, we create a dataset consisting of aperture images as the input to the model and the corresponding source contours as the output. A CNN typically requires thousands of data points to train effectively. However, only a few hundred data points are available from experiments conducted at the NIF. Therefore, we use synthetic data generated via the forward model[11] formulated in Eq. (1). This approach involves specifying the source's location and shape and then simulating its projection through the aperture array to produce an aperture image. For each simulation, we obtain a data point consisting of the aperture image and the major and minor axes parameters specifying the elliptical contour.

In general, the information provided to the reconstruction algorithm is affected by both aperture type and its pointing location. In order to compare the performance for various types of apertures, we create two separate datasets with different types of aperture projections. The first dataset consists of images with circular penumbra apertures only, as shown in Fig. 3(a). The second dataset consists of images with penumbra and triangular pinholes, as shown in Fig. 3(b). The penumbra often has much higher neutron counts per pixel due to its wide field-of-view and thus is much brighter in the image compared to the pinholes. For the penumbra models, we generate aperture images consisting of all three penumbras. For the pinhole and penumbra models, we generate all three penumbras, as well as a selection of 12 pinhole apertures. The 12 pinholes are chosen based on their pointing location in the source plane field-of-view. For the best performance, the selection of pinholes should cover as much of the field-of-view as possible. The pointing of the selected pinholes and penumbra is shown in Fig. 4. We see here that the selected pinholes cover a large portion of the field of view. In general, each additional pinhole typically allows for more accurate reconstructions by covering more of the field-of-view at the cost of additional computation time to generate the data.

We generated 10 201 data points for both the penumbra-only models, as well as the penumbra and pinhole models. We generate source ellipse sizes in 1 μm increments between 25 and 125 μm in both the horizontal and vertical direction. This results in a variety of

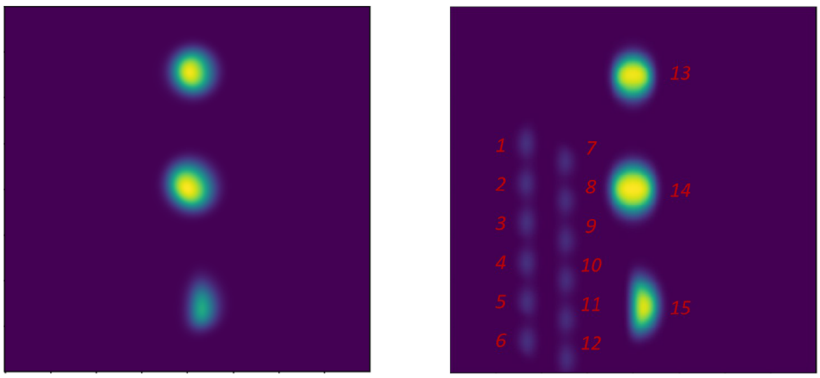

FIG. 3. Neutron aperture images for line-of-sight NIS3 generated via the forward model equation (1). (a) Only penumbra apertures are projected; (b) penumbra and a subset of 12 pinholes are projected. The number labels correspond to the labels in Fig. 4.

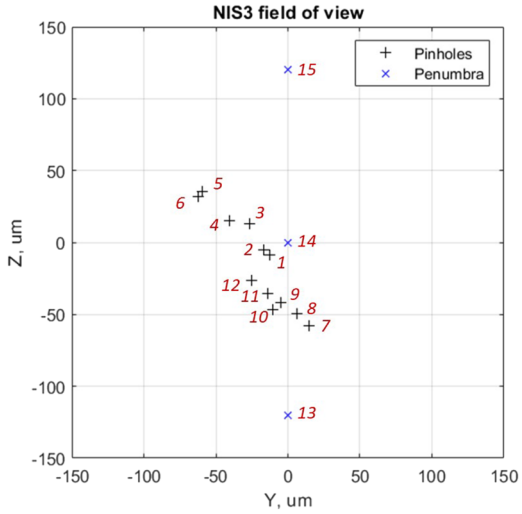

FIG. 4. Pointing location of each selected pinhole and penumbra in the source plane field-of-view for the NIS-3 line of sight at the NIF. The numbers correspond to the apertures labeled in Fig. 3(b).

sources to train and test our model, including circular, prolate, and oblate sources, as well as small and large sources.

Our data undergo several preprocessing steps before being used. First, the size of the aperture images is decreased from 1000 × 1000 pixels to 400 × 400 pixels, eliminating extraneous space and reducing the computational demands for both training and inference phases. Following this size reduction, we normalize the data using the following equation:

$$\frac{I_i - \mu}{\sigma}. \tag{2}$$

Here, I_i represents the ith aperture image in our collection, with μ and σ denoting the mean and standard deviation of all pixels across the training dataset. Considering that pixels in neutron images correspond to neutron counts, often numbering in the thousands, direct input of these images into the CNN leads to parameter explosion and training instability. Normalization adjusts the overall distribution of the training dataset to a mean of 0 and a standard deviation of 1, thus scaling pixel values down to a narrower range while preserving their distribution.

We center the images on the brightest pixel in the central penumbra and create nine additional versions of each image by applying random shifts up to 10 μm. As a result, for each aperture image, we have the original centered image along with nine altered versions. This approach enhances the model's ability to make accurate predictions even when the apertures are slightly shifted within the image.

After preprocessing, the resulting dataset contains 100 201 data points. We allocate 80% of this dataset for training purposes and the remaining 20% for testing. We also ensure that any given data point and its shifted variants are all contained within the same subset (training or testing).

B. Model and training parameters

For these experiments, we trained a CNN with 4 convolution layers with a 5 × 5 convolution filter size and 40 output channels. We apply a 2 × 2 max pooling on the output of each convolution layer. The outputs of the final convolution layer are fed into a feedforward neural network with a single hidden layer, which contains 64 nodes. The hidden layer output is fed into a final layer with two nodes. The first node predicts the horizontal axis size of the source ellipse shape, while the second node predicts the vertical axis size. The output of each convolution and hidden layer is fed through ReLU activations. We use a training batch size of 8 and trained the model for a single epoch with the ADAM optimizer[12] using a learning rate of 0.1.

We use the mean squared error loss function,

$$L = \frac{1}{n}\sum_{i=1}^{n}\left(X_i - \tilde{X}_i\right)^2, \tag{3}$$

where n is the number of training data points, X_i are the ellipse parameters predicted by the CNN, and $\tilde{X}_i$ are the ground truth ellipse parameters. In our experiments, we measure error using the Euclidean distance between the ground truth and predicted ellipse shapes. We built our CNN models using the PyTorch[13] framework.

C. Performance over various shapes

We show the results of a model trained on penumbra apertures only in Fig. 5. This heatmap shows the error of the model for various source shapes, with brighter colors indicating larger error. We see that the model only performs well for circular contours. As the contour becomes more prolate or oblate, the model error increases. Thus, these results indicate that the penumbra alone is not sufficient for determining overall source shape, especially for non-circular contours.

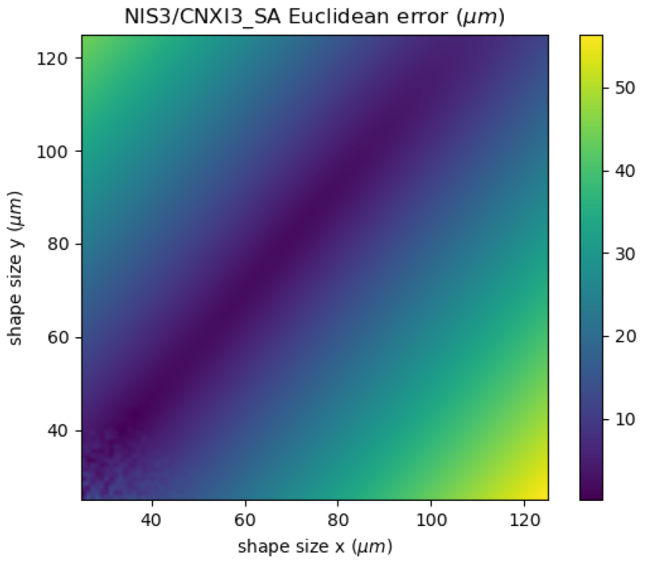

FIG. 5. Performance for CNN trained with penumbra only—heatmap shows error for various shapes and sizes of implosion. In general, the model only performs well for circular sources.

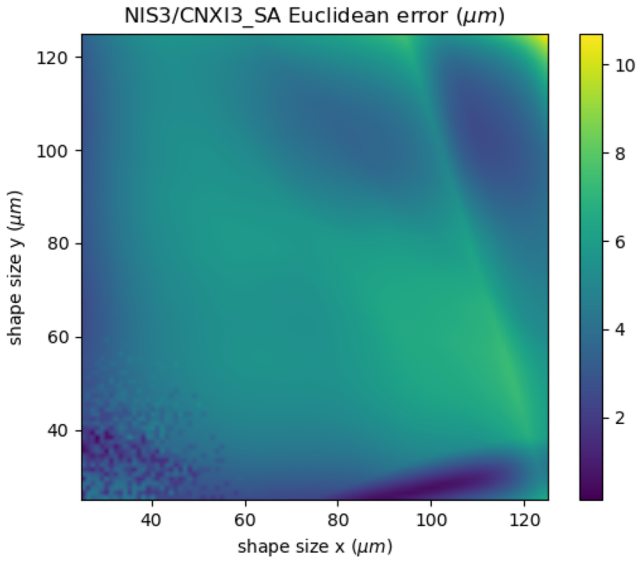

FIG. 6. Performance for CNN trained with penumbra and pinholes—heatmap shows error for various shapes and sizes of implosion. The model trained with pinholes significantly outperforms penumbra-only model and can accurately predict elliptical sources. It should be noted the color scale differs from Fig. 5 to more clearly show the differential in performance over source sizes.

The results for the model trained on penumbra and pinholes are shown in Fig. 6. We see that the performance greatly improves over the penumbra-only model. The overall error has gone down and additionally the model performs well for prolate and oblate sources. We can see that for most sources, the error is less than 6 μm. Thus, when pinholes are included, the CNN offers an accurate prediction for the elliptical contour. In addition, CNNs take only seconds to make predictions, resulting in a fast and accurate contour reconstruction.

D. Performance on noisy data

The previous experiments assumed a noise-free setting. However, noise present in experiments at the NIF can adversely affect the integrity of the aperture images, potentially leading to inaccuracies in CNN predictions. To ensure the robustness of our models, it is crucial that they maintain high performance in the presence of noise. The types of noise that typically impact the neutron imaging system are best characterized by Gaussian or Poisson distributions.[10] Figure 7 shows how CNN accuracy is affected as noise levels increase. In particular, in Fig. 7(a), Gaussian noise with a zero mean is introduced, and we observe the model's average error across 50 validation set samples as the standard deviation varies. Similarly, Fig. 7(b) shows the impact of applying a Poisson noise distribution with varying mean event numbers. The CNN shows stable performance over low levels of noise under both noise models. In addition, the model is more robust to Poisson noise compared to Gaussian noise. However, as the noise level increases, we see a sharp degradation in the CNN performance.

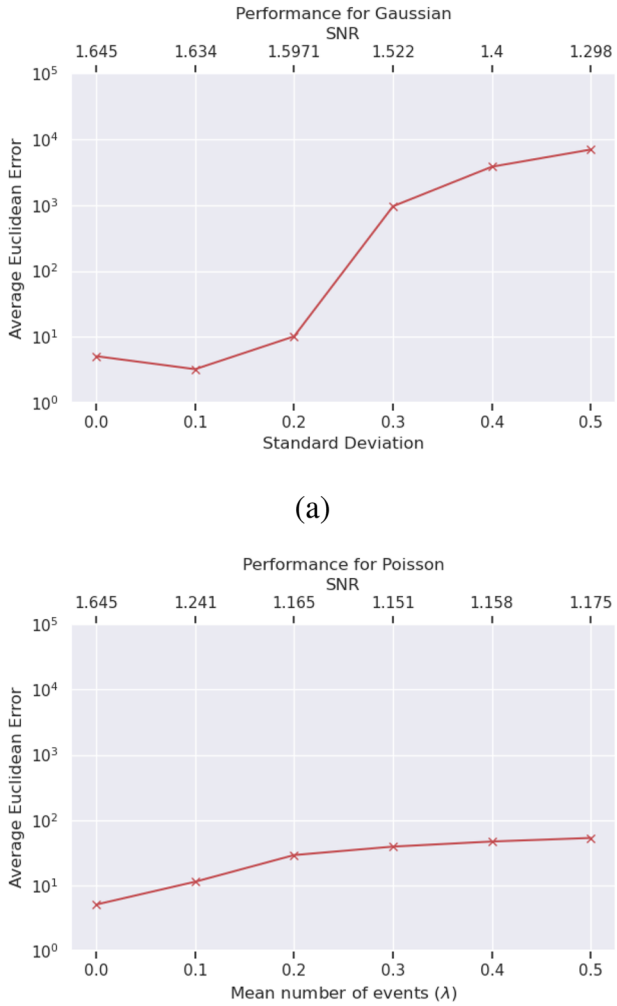

FIG. 7. Performance of a CNN trained with pinholes and penumbra for varying noise levels. (a) Gaussian noise is added; (b) Poisson noise is added. The performance is strong for small levels of noise. It should be noted that noise is applied to the normalized images whose pixel values lie heavily in a range between −1 and 1.

In order to compare the noise levels to real NIF conditions, we compute the signal-to-noise ratio (SNR) over the aperture image datasets using the following equation:

$$SNR_{avg} = \frac{1}{N}\sum_{i=1}^{N}\frac{\mu_i}{\sigma_i}, \tag{4}$$

where N is the number of aperture images in the dataset, μ_i is the mean of aperture image i, and σ_i is the standard deviation of image i. As shown in the work by Saavedra *et al.*,[14] the SNR of a typical NIF experiment is 1.636. We require that the CNN perform well at or below this SNR level. The SNR values associated with various levels of noise are plotted along the top x-axis of Fig. 7. We see

that the CNN does indeed perform well under expected NIF noise conditions.

IV. CONCLUSION

In this paper, we have shown that neural networks can accurately model the outer contour of an ICF source using elliptical approximations. In particular, we show that convolutional neural networks (CNNs) can predict these shapes using an entirely data-driven approach, i.e., with no physical knowledge of the source or aperture geometry. We also show that model accuracy is greatly improved by including pinholes in the aperture image.

There are several possibilities for future work. Currently, the CNN does not outperform traditional techniques in terms of accuracy. One possible improvement is to include additional pinholes as well as increase the amount of training data. In addition, this work used only a single CNN for prediction. However, we may obtain more accurate and robust predictions using an ensemble of models. We may also improve the performance of the model in noisy environments by incorporating noise into the training data. Finally, this work showed the feasibility of predicting source geometry characteristics using machine learning. We can further apply the methodology derived in this paper to predict more complex contours, e.g., non-elliptical contours that more accurately describe the source geometry.

ACKNOWLEDGMENTS

We thank the dedicated staff at NIF for their contributions and hard work. This work was supported by the U.S. Department of Energy through the Los Alamos National Laboratory (LANL), operated by Triad National Security, LLC, for the National Nuclear Security Administration under Contract No. 89233218CNA000001.

AUTHOR DECLARATIONS

Conflict of Interest

The authors have no conflicts to disclose.

Author Contributions

Gary Saavedra: Conceptualization (lead); Data curation (equal); Formal analysis (lead); Investigation (lead); Methodology (lead); Software (equal); Writing – original draft (lead); Writing – review & editing (lead). **Verena Geppert-Kleinrath**: Data curation (equal); Funding acquisition (equal); Project administration (equal); Software (equal). **Chris Danly**: Conceptualization (equal); Data curation (equal); Software (equal). **Mora Durocher**: Data curation (equal); Software (equal). **Carl Wilde**: Data curation (equal); Software (equal). **Valerie Fatherley**: Data curation (equal). **Emily Mendoza**: Data curation (equal). **Landon Tafoya**: Data curation (equal). **Petr Volegov**: Conceptualization (equal); Data curation (equal); Software (equal). **David Fittinghoff**: Data curation (equal); Project administration (equal). **Michael Rubery**: Data curation (equal). **Matthew S. Freeman**: Data curation (equal); Project administration (lead); Software (equal).

DATA AVAILABILITY

The data that support the findings of this study are available from the corresponding author upon reasonable request.

REFERENCES

[1] H. Abu-Shawareb, R. Acree, P. Adams, J. Adams, B. Addis, R. Aden, P. Adrian, B. Afeyan, M. Aggleton, L. Aghaian *et al.*, "Lawson criterion for ignition exceeded in an inertial fusion experiment," Phys. Rev. Lett. **129**, 075001 (2022).
[2] F. Merrill, D. Bower, R. Buckles, D. Clark, C. Danly, O. Drury, J. Dzenitis, V. Fatherley, D. Fittinghoff, R. Gallegos *et al.*, "The neutron imaging diagnostic at NIF (invited)," Rev. Sci. Instrum. **83**, 10D317 (2012).
[3] V. Geppert-Kleinrath, M. S. Freeman, C. R. Hurlbut, F. Merrill, J. R. Tinsley, P. Volegov, and C. Wilde, "A liquid VI scintillator cell for fast-gated neutron imaging," Rev. Sci. Instrum. **89**, 10I142 (2018).
[4] P. Volegov, C. Danly, D. Fittinghoff, G. Grim, N. Guler, N. Izumi, T. Ma, F. Merrill, A. Warrick, C. Wilde, and D. C. Wilson, "Neutron source reconstruction from pinhole imaging at National Ignition Facility," Rev. Sci. Instrum. **85**, 023508 (2014).
[5] J. Valente, J. António, C. Mora, and S. Jardim, "Developments in image processing using deep learning and reinforcement learning," J. Imaging **9**, 207 (2023).
[6] N. O'Mahony, S. Campbell, A. Carvalho, S. Harapanahalli, G. V. Hernandez, L. Krpalkova, D. Riordan, and J. Walsh, "Deep learning vs. traditional computer vision," in *Advances in Computer Vision: Proceedings of the 2019 Computer Vision Conference (CVC)* (Springer, 2020), Vol. 11, pp. 128–144.
[7] L. Nanni, S. Ghidoni, and S. Brahnam, "Handcrafted vs. non-handcrafted features for computer vision classification," Pattern Recognit. **71**, 158–172 (2017).
[8] W. Lin, K. Hasenstab, G. Moura Cunha, and A. Schwartzman, "Comparison of handcrafted features and convolutional neural networks for liver MR image adequacy assessment," Sci. Rep. **10**, 20336 (2020).
[9] I. Goodfellow, Y. Bengio, and A. Courville, *Deep Learning* (MIT Press, 2016).
[10] P. Volegov, C. Danly, D. Fittinghoff, N. Guler, F. Merrill, and C. Wilde, "Self characterization of a coded aperture array for neutron source imaging," Rev. Sci. Instrum. **85**, 123506 (2014).
[11] D. Wilson, G. Grim, I. Tregillis, M. Wilke, M. Patel, S. Sepke, G. Morgan, R. Hatarik, E. Loomis, C. Wilde *et al.*, "Modeling the National Ignition Facility neutron imaging system," Rev. Sci. Instrum. **81**, 10D335 (2010).
[12] D. P. Kingma and J. Ba, "Adam: A method for stochastic optimization," arXiv:1412.6980 (2014).
[13] A. Paszke, S. Gross, F. Massa, A. Lerer, J. Bradbury, G. Chanan, T. Killeen, Z. Lin, N. Gimelshein, L. Antiga *et al.*, "PyTorch: An imperative style, high-performance deep learning library," in *Advances in Neural Information Processing Systems 32 (NeurIPS 2019)* (NeurIPS, 2019).
[14] G. Saavedra, V. Geppert-Kleinrath, C. Danly, M. Durocher, C. Wilde, V. Fatherley, E. Mendoza, L. Tafoya, P. Volegov, D. Fittinghoff *et al.*, "Source localization for neutron imaging systems using convolutional neural networks," Rev. Sci. Instrum. **95**, 063503 (2024).